

Experimental Charge Density Analysis of the Anti-inflammatory Drug Meloxicam [sodium 4-hydroxy-2-methyl-*N*-(5-methyl-1,3-thiazol-2-yl)-1,1-dioxo-1 λ ^6,2-benzothiazine-3-carboxamide Monohydrate]

Niranjana Devi Rajendran,¹ Arputharaj David Stephen,^{2,*} Christian Jelsch,³ Eduardo C. Escudero-Adán⁴

¹ Department of Physics, Fatima College, Madurai, Tamil Nadu, India

² Department of Physics, Sri Shakthi Institute of Engineering and Technology, Coimbatore, Tamil Nadu, India

³ CRM2, UNR CNRS 7036, Institut Jean Barriol, Université de Lorraine, Vandoeuvre les Nancy cedex, France

⁴ The Barcelona Institute of Science and Technology, Institute of Chemical Research of Catalonia (ICIQ), Av. Països Catalans 16 - 43007 Tarragona, Spain

* Corresponding author's e-mail address: davidstephen_dav@yahoo.co.in

RECEIVED: April 14, 2018 * REVISED: May 16, 2018 * ACCEPTED: May 23, 2018

THIS PAPER IS DEDICATED TO DR. BISERKA KOJIC-PRODIC ON THE OCCASION OF HER 80TH BIRTHDAY

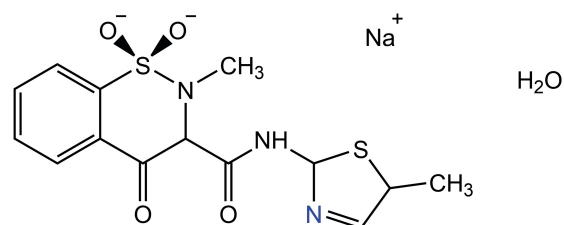
Abstract: The charge density analysis of meloxicam sodium monohydrate [sodium 4-hydroxy-2-methyl-*N*-(5-methyl-1,3-thiazol-2-yl)-1,1-dioxo-1 λ ^6,2-benzothiazine-3-carboxamide monohydrate] was performed with high-resolution X-ray diffraction data measured at low temperature (90 K). The experimental results were compared with those derived from the corresponding periodic theoretical calculations at the B3LYP/6-31G** level of theory. The multipolar charge-density analysis highlights the regions of meloxicam which are the most electronegative. These regions correspond to those forming short electrostatic interactions with the Na⁺ cation.

The molecular conformation in the crystal is maintained by a strong intramolecular N–H···O=C hydrogen bond. The Na⁺ cation interacts with as much as five neighboring oxygen atoms. The strong hydrogen bonds N/O–H···O/N, the Na⁺···O short contacts and hydrophobic aromatic stacking between the two aromatic cycles constitute the most represented and enriched contact types and act as the driving force in the crystal packing formation. The crystal packing presents several meloxicam anion dimers but also one Na⁺···Na⁺ repulsive interactions which are largely compensated by the electrostatic favorable attractions between anions and cations.

Keywords: meloxicam, X-ray crystallography, quantum calculation, electron density, topological analysis, electrostatic potential, interaction energy.

HEADING 1

MELOXICAM [sodium 4-hydroxy-2-methyl-*N*-(5-methyl-1,3-thiazol-2-yl)-1,1-dioxo-1 λ ^6,2-benzothiazine-3-carboxamide monohydrate] (Scheme 1) is a nonsteroidal anti-inflammatory drug (NSAID) with analgesic and fever reducer effects comes under the enolic-acid group of NSAIDs. Meloxicam blocks cyclooxygenase (COX), the enzyme accountable for changing arachidonic acid into prostaglandin H₂, which is the first step in the synthesis of prostaglandins and acts as arbitrator of inflammation. The



Scheme 1. Sodium 4-hydroxy-2-methyl-*N*-(5-methyl-1,3-thiazol-2-yl)-1,1-dioxo-1 λ ^6,2-benzothiazine-3-carboxamide monohydrate.

peculiar effect of meloxicam was reflected from the inhibition with COX-2 over COX-1 at low therapeutic doses.^[1]

In the effective treatment of osteoarthritis, meloxicam has been utilized since 2000.^[2,3] Commonly the NSAIDs are useful in treating the inflammation and pain associated with rheumatic diseases.^[4] As the chemical structures of NSAIDs are different from steroidal drugs, the term “non-steroidal” is used and they possess anti-inflammatory activity.^[5] In a wide range, NSAIDs are inhibitors of prostaglandin H synthase also known as cyclooxygenase (COX). The identified two COX isoenzymes COX-1 and COX-2 are present in all tissues, cell types, especially platelets, endothelial cells, renal micro vasculature, glomerulus and collecting ducts. Moreover, the COX-1 protein is responsible for the production of prostaglandins that are essential for homeostatic activities whereas COX-2 is considered as an inducible iso-enzyme and also takes a major role in pain and inflammatory processes.

Some NSAIDs such as aspirin, ketoprofen, indomethacin, piroxicam, sulindar are mainly selective for COX-1 and some such as ibuprofen, naproxen, diclofenac are slightly selective for COX-1 and some like etadolac, nabumentone and meloxicam are slightly selective for COX-2 and some like celecoxib and rofecoxib are primarily selective for COX-2.

Notably, meloxicam has a weak effect on gastric acid secretion and on ulceration in rat stomach when it is compared with other NSAIDs. Meloxicam exhibits preferential inhibition of COX-2 over COX-1 with good gastric and renal tolerability. It has less photo toxicity than diclofenac, lectoprofen and naproxen. It also shows a high potency in animal tests for potential anti-arthritis action and anti-inflammatory activity along with reduced gastric irritation and local tissue irritation compared to other NSAID drugs.

Meloxicam has a good bio-availability (89 %) and very low oral toxicity of high doses. On satisfying the Lipinski rule of five parameters, the meloxicam sodium monohydrate salt proves itself as an effective drug. The molecular properties such as $\log P = 2.24$, molecular weight = 351.41 g/mol, seven hydrogen bond donors, two hydrogen bond acceptors and two rotatable bonds were strongly associated with the solubility and permeability.

In this work, the experimental electron density of the meloxicam sodium monohydrate has been carried out with high-resolution X-ray data collection at 90 K. The bonding details, topological, enrichment contacts, electrostatic properties and quantum chemical properties have been calculated to retrieve the intricate details of the molecule at subatomic level and interactions in the crystal packing.

MATERIALS AND METHODS

Crystallization

Crystals of meloxicam sodium monohydrate were grown by slow evaporation from a saturated aqueous and methanol solution at room temperature. A high quality single crystal was selected for high resolution X-ray diffraction intensity measurements.

X-ray Data Collection and Structure Solution

Single-crystal X-ray high-resolution and highly redundant data collection of meloxicam sodium monohydrate compound was performed on a Rigaku Micro Max-HF rotating anode diffractometer equipped with a Pilatus 200K hybrid pixel detector using MoK α radiation. The data collection was carried out at 90(2) K under a stream of nitrogen using the Oxford 700 Plus Cryo-systems gas flow apparatus. Data reduction and absorption correction were performed using the CrysAlisPro 1.171.39.12f package,^[6] the internal $R(I)$ factor was 4.4 % for all reflections.

The crystal was mounted using a capton micro-loop. A high resolution data set was collected upto $(\sin \theta / \lambda)_{\max} = 1.2 \text{ \AA}^{-1}$, the completeness being 98 % at $\sin \theta / \lambda = 1.11 \text{ \AA}^{-1}$. The unit cell parameters refinement, data reduction and absorption correction have been carried out using 1.171.39.12f package.^[6] For data averaging the program XPREP Version 2014/02 has been used.^[7] Molecular graphics has been computed using Olex2.^[8] The structure has been solved with the SIR2014,^[9] structure solution program using VLD algorithm and refined with the ShelXTL Version 2014/7^[10] under the ShelXle interface.^[11] Further details of crystal data and measurement conditions are given in Table 1.

Multipolar Experimental Refinement

The experimental electron density distribution was performed with the help of multipolar atom formalism^[12] incorporated in the MoPro Software^[13] which has been utilized to estimate the electron density distribution of small molecules from high resolution X-ray single crystal diffraction data.

The core and valence spherical scattering factors were calculated using the wave functions for isolated atoms from Su and Coppens^[14] and the anomalous dispersion coefficients were taken from Kissel *et al.*^[15] The charge density was refined against diffraction intensities truncated at $s < 1.2 \text{ \AA}^{-1}$. For the H atoms, the values of anisotropic U_{ij} thermal parameters were fixed to those obtained from the SHADE3 server.^[16] The H–X distances of H atoms were restrained to the values obtained from neutron diffraction studies^[17] with a restraint sigma σ_d of

Table 1. Experimental details of crystal and X-ray diffraction data collection

Crystal data	
Chemical formula	C ₁₄ H ₁₄ N ₃ Na O ₅ S ₂
Formula weight	391.386
Crystal system, space group	<i>P</i> $\bar{1}$
Temperature (K)	90(2)
<i>a</i> , <i>b</i> , <i>c</i> (Å)	8.3990(10), 9.44910(10), 11.09693(10)
α , β , γ	78.473(10), 73.257(10), 69.435(10)
<i>V</i> (Å ³)	784.812(14)
<i>Z</i>	2
Crystal size (mm)	0.1 × 0.05 × 0.05
Radiation	MoK α
absorption μ (mm ⁻¹)	0.400
Diffractometer	Rigaku MicroMax-007HF
<i>T</i> _{min} , <i>T</i> _{max}	0.982, 0.991
Measured reflections	91508
Independent reflections	20997
<i>R</i> _{int} , <i>R</i> _{sigma}	0.0278, 0.0250
sin θ _{max} / λ (Å ⁻¹)	1.20
$\Delta\rho$ _{max} , $\Delta\rho$ _{min}	-0.42 °; 0.64
Refinement (multipolar)	
No. of reflections	20997
<i>R</i> (<i>F</i>) (%)	2.8
<i>wR</i> ² (<i>I</i>) (%)	3.3

0.01 Å. Distance X–H similarity restraints were also applied to chemically equivalent groups.

The S atoms were treated up to hexadecapole level, the C,N,O atoms up to octapole level, the H atoms with one dipole among H–X bond, while the Na cation was set to monopolar with a charge of +1e.

For the water molecule, local symmetry constraint was applied to the multipoles of the oxygen atom and the two H atoms were set equivalent. The charge density of the water atoms was restrained ($\sigma_r = 0.01$) to that of the ELMAM2 databank.^[18] The hydrogen atoms of water molecule were set isotropic with $U_{iso}=1.5U_{eq}(O)$ riding on the equivalent B-factor of the oxygen atom.

For the non-H atom, enhanced rigid-bond restraints^[19] were applied on the anisotropic thermal parameters. Expansion/contraction coefficients κ and κ' of H atoms were restrained to be similar ($\sigma = 0.001$). Chemical equivalence and local symmetry restraints were applied on atoms with highest thermal motion (O1 ≈ O2, CH₃ groups). The different structural and charge density parameters were refined iteratively till convergence.

In order to ensure the neutrality of the molecule during the refinement, the electro-neutrality constraint was applied through the refinement. The correctness of the model was confirmed by the featureless residual density map which was generated by the VMoPro module. The bond-topological properties such as electron density, the

Laplacian of the electron density, the bond ellipticity and the atomic charges were estimated by VMoPro. The variation of scale factor $\Sigma(F_o^2) / \Sigma(F_c^2)$, with respect to resolution for the meloxicam sodium monohydrate molecule is given in Sup. Figure 1. The normal probability plot of $F_o^2 - F_c^2$ and the evolution of $\langle F_o^2 \rangle / \langle F_c^2 \rangle$ as a function of reciprocal resolution obtained from program DRKplot^[20] are shown in Supplementary materials (Supplementary Figure 2). The fractal dimension vs. Fourier residual electron density $F_o - F_c$ using all reflections map is shown in Supplementary Figure 3.

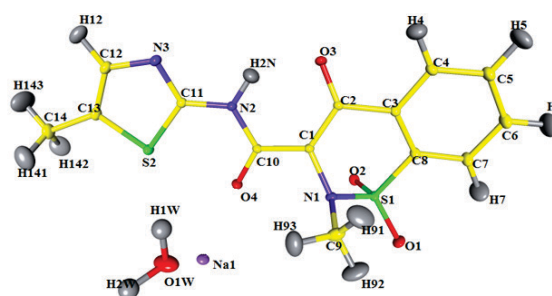


Figure 1. ORTEP view of the meloxicam sodium molecule, showing the atom-numbering scheme. Displacement ellipsoids are drawn at the 50 % probability level and H atoms are shown as small spheres of arbitrary radii.

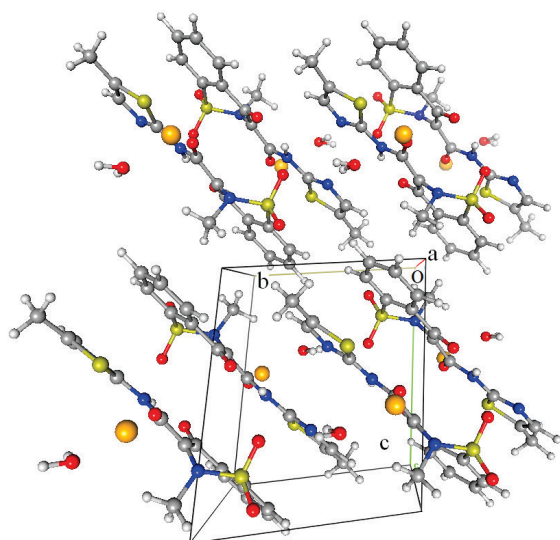


Figure 2. Autostereogram (Katrusiak, 2001) showing the crystal packing of meloxicam sodium monohydrate along a axis.

Theoretical Calculations

On the basis of Kohn-Sham^[21,22,23] wave-functions, the analysis of the molecule meloxicam sodium monohydrate had been done. The minimum energy structure and corresponding electronic wave functions of the molecule meloxicam sodium monohydrate had been obtained using the Kohn-Sham computations followed by geometry optimization incorporating the B3LYP/6-311G++(d,p)^[24,25] level of theory. The software GAUSSIAN09 package^[26] was utilized for this purpose. The absence of imaginary frequencies confirmed that they correspond to real minima. The electronic wave functions had been generated from GAUSSIAN09 which served as the input for the AIMALL program^[27] in order to explore the bond topological and electrostatic features at the bond critical point.

RESULTS AND DISCUSSION

Structure Description

The crystal structure of meloxicam sodium monohydrate at 90(2) K obtained in this study (Figure 1), agrees well with the equivalent structure obtained at room temperature.^[28] The experimental bond lengths, angles and torsion angles are given in the supplementary tables. The N3 atom belongs to a flat five-membered ring geometry [C11–N3–C12 = 110.03 °(2)]. N3 atom forms two covalent bonds with C11 and C12 atoms leaving lone pairs in the sp^2 plane. The lengths of N–C bonds show the occurrence of resonance or delocalization among the bonds. However, the N1–C1 bond is longer than other N–C bonds at $d =$

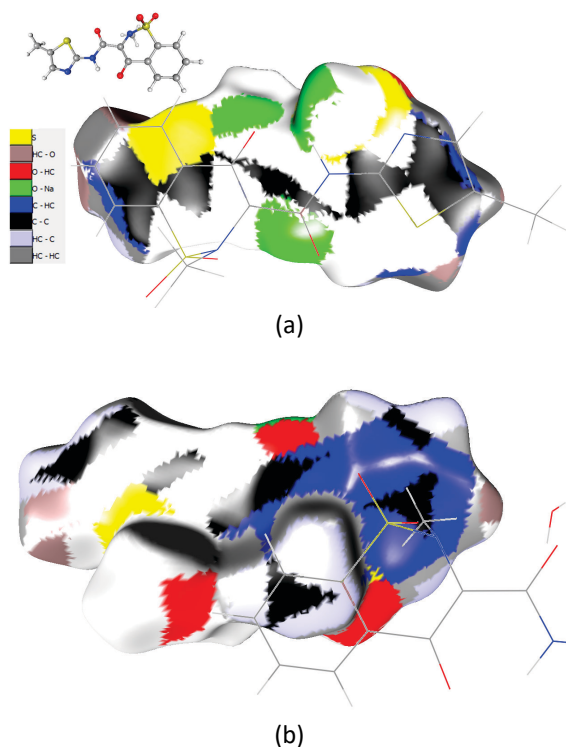


Figure 3. View of the Hirshfeld surface the meloxicam molecule coloured according to the main contact types. (a) front view, orientation of the M molecule is shown in ball and sticks (b) rear view obtained by 180° rotation around horizontal axis.

1.445(2) Å as C1 and N1 atom are both in sp^3 hybridization. The N1 atom has a tetrahedral geometry but the three angles $S1-N1-C9 > C1-N1-C9 > S1-N1-C1 = 113.997(10)^\circ$ are all greater than the ideal value of 109° . Both C=O bonds enunciate a double bond character and they have lengths of $C10-O4 = 1.2499(2) \text{ \AA}$ and $C2-O3 = 1.2691(2) \text{ \AA}$.

The compound bears a SO_2 group; the geometry associated with the S1 atom is tetrahedral and the hybridization connected with the S1 atom is sp^3 . The smallest and largest angles involving the S atom are $C11-S2-C13 = 89.745(10)^\circ$ and $O1-S1-O2 = 118.23(2)^\circ$.

The $O4-C10-N2$ angle in the amide planar part is calculated as $120.773(13)^\circ$ which suggests a trigonal planar geometry and the sp^2 hybridization state for the corresponding central carbon atom C10.

Packing and Interactions

The packing of the molecule is mainly stabilized by contacts such as $C-H\cdots O$, $N-H\cdots C$, $N-H\cdots O$, $O-H\cdots O$, $O-H\cdots C$ and $O-H\cdots N$. The hydrogen bonding geometry is listed in Table 2. The intramolecular contact $N2-H2N\cdots O3$ and the intermolecular contact $O1W-H1W\cdots N3$ are having short $H\cdots A$ distances of $1.902(5) \text{ \AA}$ and $1.914(5) \text{ \AA}$ and Laplacian values

Table 2. Hydrogen-bond geometry (\AA , $^\circ$)

D-H...A	D-H (\AA)	H...A (\AA)	D...A (\AA)	D-H...A ($^\circ$)
O1W-H2W...O2	0.955	2.434	3.0401(2)	121.2(4)
C14-H143...O1	1.070	2.551	3.3135(3)	127.5(3)
N2-H2N...C2	0.993	2.471	2.8881(2)	104.8(3)
N2-H2N...O3	0.993	1.902	2.6938(2)	134.6(3)
C9-H92...O1	1.057	2.394	2.8649(3)	105.6(3)
C14-H142...O1	1.058	2.623	3.4482(3)	134.5(3)
O1W-H1W...C12	0.956	2.710	3.4932(3)	139.6(3)
O1W-H1W...N3	0.956	1.914	2.8559(3)	168.09(15)
N2-H2N...O2	0.993	2.526	3.1916(2)	124.2(3)

of $3.32 \text{ e}/\text{\AA}^5$ and $1.47 \text{ e}/\text{\AA}^5$ respectively. The crystal packing of meloxicam sodium monohydrate along a axis takes the shape of zigzag structures (Figure 2). The Hirshfeld surface analysis shows the nature of intermolecular interactions through the colouring scheme (Figure 3). Meloxicam has 3 regions on the molecular surface where $\text{O}\cdots\text{Na}$ interactions occur (shown in green in Figure 3a).

As seen in many other molecules^[29,30,31,32] the proportion of H...H contacts exhibit the highest percentage nearly 41.8 % in the fingerprint plot (Figure 4a). The $\text{O}\cdots\text{H}/\text{H}\cdots\text{O}$ contacts show the next highest contact surface reaching 16.8 % (Figure 4b).

In Table 3, the contact types on the Hirshfeld surface and their enrichment are displayed. The contact enrichment ($E_{xy} = C_{xy}/R_{xy}$) is the ratio between actual contacts and equiprobable (random) contacts which are computed from the surface composition.^[33] The Hirshfeld surface was generated around meloxicam, Na^+ and HOH moieties not in contact with each other in the crystal in order to obtain

three integral surfaces. The hydrophobic atoms C and Hc (H bound to C) represent more than half of the global Hirshfeld surface at 53.8 % while Hc atoms occupy nearly a third of the surface. As a consequence hydrophobic contacts, such π -stacking and $\text{C-H}\cdots\pi$ interactions involving C and Hc atom types are major interactions and represent as much as 40 % of the whole contact surface. $\text{C-H}\cdots\pi$ interactions occur notably between the methyl group and the C6 aromatic ring. All these contacts are enriched, notably $\text{Hc}\cdots\text{C}$ and $\text{C}\cdots\text{C}$ which display $E = 2.0$ and 1.8 respectively.

Among the polar interactions, there are three $\text{O}\cdots\text{Na}^+$ ionic bridges (Figure 3a) which represent a major contact reaching 14.8 % in proportion and is the most over-represented contact in the crystal packing at $E = 3.8$. The strong hydrogen bonds $\text{O}\cdots\text{Hn/o}$ are, as expected, over-represented, but the $E = 1.38$ value is relatively moderate, presumably due to competition with the more energetic $\text{O}\cdots\text{Na}^+$ ionic bridges. Conversely, the sulphur atoms, which constitute a weaker hydrogen bond acceptor compared to

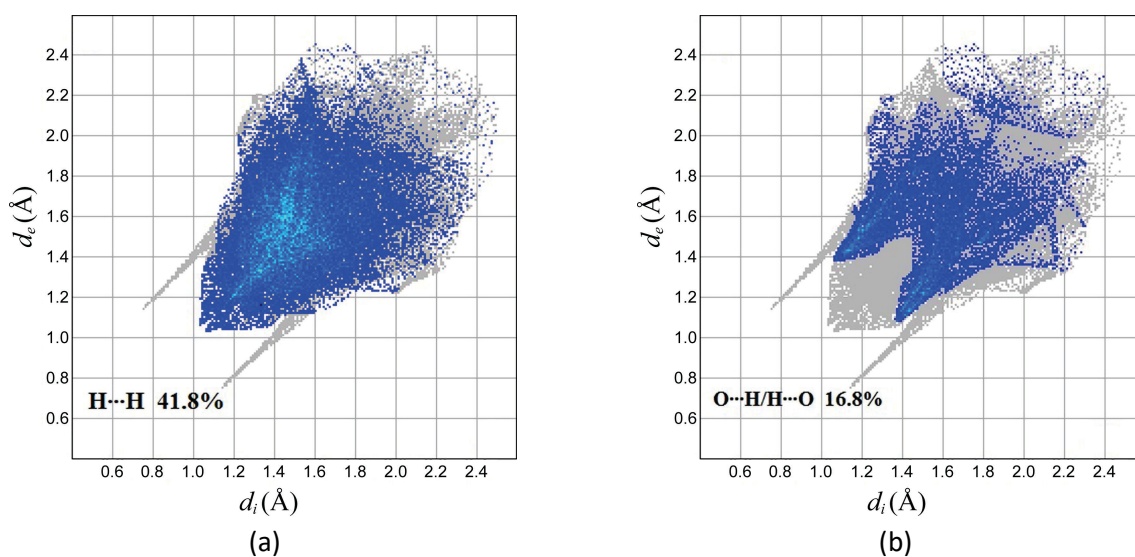
**Figure 4.** Fingerprint plots: resolved into a) H...H contacts (b) O...H contacts showing the percentages of contact contributing to the total Hirshfeld surface area of the meloxicam sodium molecule in the crystal.

Table 3. Chemical proportions on the Hirshfeld surface of the three entities: meloxicam, Na⁺ and HOH. Contacts types and their enrichment in the crystal of the title compound are also given. Hydrophobic Hc hydrogen atoms bound to carbon are distinguished from the polar ones Hn/o in H–N and HOH moieties. The major and most enriched contacts are highlighted in bold characters

atom	Hn/o	C	N	O	Na	S	Hc
surf %	8.6	21.7	4.4	16.7	8.4	8.0	32.2
Hn/o	0.8						
C	1.4	8.3		Actual	Contacts	%	
N	3.0	3.5	0.1				
O	3.4	0.9	0.5	0.1			
Na	1.5	2.0	0.7	14.8	0.4		
S	3.9	3.0	0.7	2.0	2.4	1.3	
Hc	2.1	13.8	0.0	8.1	2.9	0.4	18.3
Hn/o	1.12						
C	0.40	1.96		Enrichment			
N	4.19	1.98	0.41				
O	1.38	0.15	0.43	0.03			
Na	0.70	0.38	0.62	3.83	0.26		
S	3.10	0.99	1.10	0.90	1.25	2.28	
Hc	0.38	1.05	0.00	0.85	0.36	0.09	1.79

O=C and O=S oxygen, have very enriched S...Hn/o contacts at $E = 3.1$. The O...Hc contacts are also more favored ($E = 1.8$) than the O...Hn/o hydrogen bonds as the SO₂ group turns out to interact with two CH₃ groups.

Charge Density and Topology of the Covalent Bonds

The featureless Fourier residual density map drawn at resolution $0.42 \text{ \AA} < d < 7.69 \text{ \AA}$ in the benzene ring plane shows the quality of the data as well as the efficiency of the multipole model (Supplementary Figure 4). The static deformation density maps for the planes C11–S2–C13 and O1–S1–O2 in Figure 5 clearly shows the bonding regions as well as the lone pairs of O1 and O2 atoms. The three dimensional static deformation density maps of meloxicam sodium monohydrate are shown in Figure 6. The Laplacian maps (Figure 7) shows the charge concentration and depletion regions for the planes C11–S2–C13 and O1–S1–O2.

The topological properties of covalent bonds are tabulated in Table 4 as well as in the supplementary tables. As seen in the molecules such as rhodanine and 2,4-thiazolidinedione^[34] the S1–O1 and S1–O2 bonds show positive Laplacian values (9.06 e/\AA^5 and 4.93 e/\AA^5) at the bond CPs typically. The electron density values are however high (2.26 e/\AA^3 and 2.31 e/\AA^3). Among the N–C bonds, the N3–C11 bond shows the highest Laplacian values (-25.0 e/\AA^5) and has the shortest length $d = 1.3089(3) \text{ \AA}$; it shows the highest concentration of charges along the bond path as well as the shared shell interaction.

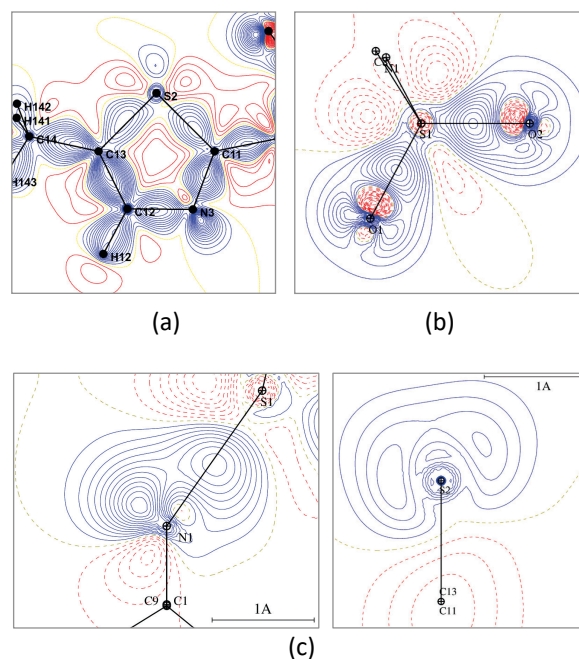


Figure 5. Deformation electron density map in the (a) C11–S2–C13 and (b) O1–S1–O2 planes of the meloxicam molecule. (c) View of N1 nitrogen electron lone pair in the plane containing the N1–S1 bond and bisecting C1–N1–C0. (d) View of the S2 sulphur lone pairs in the plane bisecting C13–S1–C11. Contour intervals are 0.05 e/\AA^3 ; blue lines represent positive contours, red lines are negative contours and the yellow lines are zero contours.

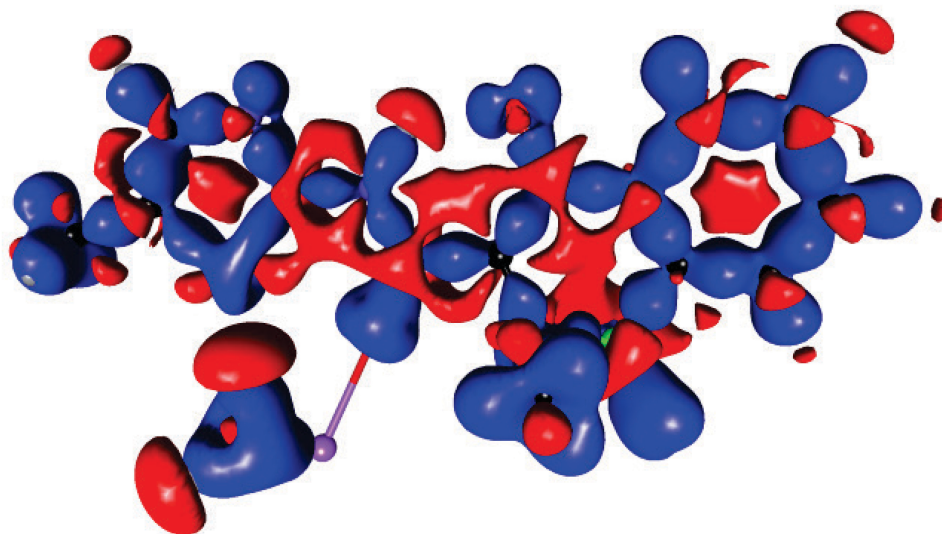


Figure 6. Three dimensional static deformation density map of the meloxicam Sodium monohydrate compound. The isosurfaces are drawn at the intervals of $0.05 \text{ e}/\text{\AA}^3$. Positive and negative values are represented in blue and red, respectively. The orientation of the molecule is the same as in Figure 1.

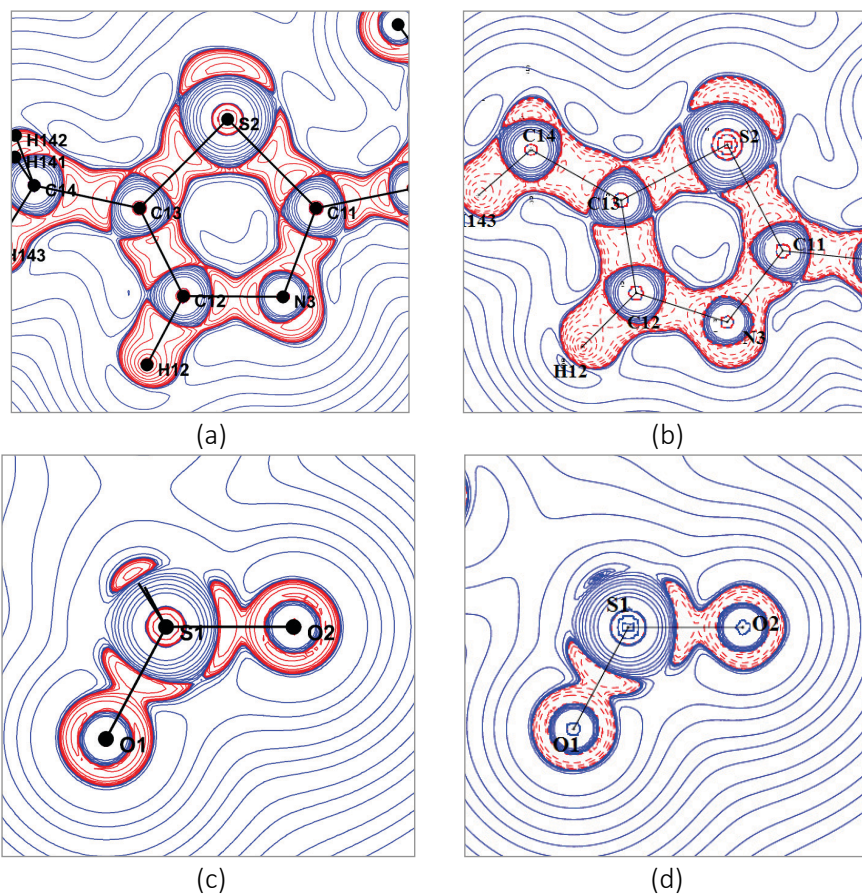


Figure 7. Laplacian of the electron density in the C11–S2–C13 plane a) EXP b) THEO and O1–S1–O2 plane a) EXP b) THEO. Solid blue and red lines represent the positive and negative contour lines respectively. Contour level $2, 4, 8, 10^n$, $n = -1, 0, 1$.

Table 4. Topological properties at the critical points of covalent bonds: electron density, Laplacian and ellipticity, ϵ . 1st line: experimental, 2nd line: theoretical

Bonds	ρ (e/Å ³)	$\nabla^2\rho$ (e/Å ⁵)	ϵ	d_1 (Å)	d_2 (Å)	R_{ij} (Å)
C1–N1	1.77	–10.6	0.129	0.618	0.826	1.444
	1.76	–15.1	0.137	0.550	0.896	1.446
C9–N1	1.66	–7.8	0.043	0.633	0.836	1.469
	1.71	–15.1	0.044	0.590	0.880	1.470
C10–N2	2.17	–21.7	0.176	0.551	0.817	1.368
	2.12	–21.7	0.114	0.506	0.862	1.368
C11–N2	2.13	–19.8	0.256	0.582	0.796	1.378
	2.09	–22.1	0.177	0.847	0.531	1.379
C11–N3	2.51	–25.0	0.256	0.560	0.748	1.309
	2.47	–26.4	0.239	0.507	0.803	1.310
C12–N3	2.19	–16.7	0.127	0.606	0.774	1.380
	2.11	–21.8	0.113	0.849	0.532	1.381
C2–O3	2.53	–29.2	0.113	0.474	0.795	1.269
	2.46	–11.4	0.040	0.439	0.830	1.269
C10–O4	2.65	–26.8	0.059	0.444	0.806	1.249
	2.53	–7.97	0.038	0.428	0.822	1.250
C8–S1	1.53	–10.7	0.069	0.801	0.951	1.752
	1.50	–11.7	0.065	0.943	0.810	1.752
C11–S2	1.38	–6.5	0.475	0.858	0.877	1.734
	1.42	–9.7	0.264	0.892	0.843	1.736
C13–S2	1.38	–5.6	0.337	0.809	0.924	1.731
	1.43	–9.7	0.225	0.913	0.819	1.732
N1–S1	1.75	–9.1	0.158	0.998	0.624	1.621
	1.68	–5.5	0.133	0.627	0.995	1.622
O2–S1	2.31	4.9	0.068	0.859	0.580	1.439
	2.04	28.0	0.007	0.874	0.564	1.439
O1–S1	2.27	9.1	0.058	0.857	0.576	1.433
	2.05	29.7	0.027	0.870	0.563	1.433

Topology of Intermolecular Interactions

A detailed topological analysis of the hydrogen bonding interaction and other Na \cdots O interactions has been carried out in order to elucidate the nature and strength of the interactions which are found useful in molecular recognition.^[35,36] The critical points of the strongest interactions in the crystal are shown in Table 5. All the five Na \cdots O interactions are shorter 2.64 Å which is more than

one angstrom shorter than the sum of van der Waals radii (2.27 + 1.52 = 3.79 Å). The Na \cdots O distances are on the other hand close to the sum of covalent radii (1.66 + 0.66 = 2.32 Å). The Na⁺ cation forms the shortest ionic bridges with the two carbonyl C=O atoms resulting in similar topological properties.

More detailed information regarding the relationship between the kinetic energy density G_{cp} and potential energy density V_{cp} had been retrieved from the local

Table 5. Topological properties at the critical points of the main intermolecular interactions. Electron density, Laplacian, G_{cp} and V_{cp} are the kinetic and potential energy density at the CP in kJ/mol/Bohr³

Interactions	symmetry ^(b)	G_{cp}	V_{cp}	distance / Å	d_{1cp} / Å	d_{2cp} / Å	ρ_{cp} (e/Å ³)	$\nabla^2\rho_{cp}$ (e/Å ⁵)
H1W \cdots N3	(i)	46.4	–52.5	1.914(9)	0.648	1.266	0.189	1.47
H2N \cdots O2	(i)	14.6	–9.6	2.526(11)	1.088	1.506	0.041	0.72
H143 \cdots O1	(ii)	16.7	–12.0	2.551(10)	1.451	1.130	0.054	0.79
H142 \cdots O1	(iii)	12.8	–8.6	2.623(9)	1.134	1.512	0.040	0.62
H2N \cdots O3	(iv)	72.9	–60.3	1.901(10)	0.715	1.212	0.167	3.14
O1W \cdots O2 ^(a)	(v)	19.5	–13.0	3.0401(6)	1.6007	1.458	0.050	0.96
Na1 \cdots O3	(v)	67.7	–46.9	2.2957(4)	1.057	1.239	0.116	3.25
Na1 \cdots O4	(iv)	67.5	–46.9	2.2964(5)	1.057	1.239	0.117	3.24
Na1 \cdots O1W	(iv)	64.0	–43.9	2.3377(5)	1.063	1.274	0.110	3.09
Na1 \cdots O2	(iii)	47.6	–31.5	2.4156(4)	1.101	1.315	0.085	2.34
Na1 \cdots O4	(iii)	23.7	–14.5	2.6499(5)	1.188	1.462	0.045	1.28

^(a) CP search on H2W \cdots O2 hydrogen bond leads to a bond path between O1W and O2.

^(b) Symmetry operators applying on second atom: (i) $-X+2$; $-Y+1$; $-Z+1$, (ii) $X,Y-1,Z+1$, (iii) $-X+1$; $-Y+2$; $-Z+1$, (iv) X, Y, Z , (v) $X-1, Y, Z$.

Table 6. Experimental and theoretical atomic charges Q (electrons)

Atom	Experimental	Theoretical	Atom	Experimental	Theoretical
C1	0.196	0.22	S1	2.952	3.06
C2	0.775	0.84	S2	-0.006	0.18
C3	-0.059	-0.02	H2N	0.468	0.50
C4	-0.154	0.00	H4	0.094	0.07
C5	-0.059	0.02	H5	0.151	0.00
C6	-0.084	0.00	H6	0.114	0.02
C7	-0.066	0.00	H7	0.084	0.06
C8	-0.224	-0.17	H12	0.205	0.05
C9	-0.048	0.32	H141	0.113	-0.03
C10	1.298	1.28	H142	0.142	-0.03
C11	0.724	0.84	H143	0.105	-0.01
C12	0.164	0.40	H91	0.141	0.01
C13	-0.277	-0.21	H93	0.136	0.00
C14	-0.148	0.15	H92	0.154	0.04
O1	-1.351	-1.34	N1	-1.274	-1.18
O2	-1.389	-1.31	N2	-0.961	-1.05
O3	-0.971	-1.12	N3	-0.872	-1.31
O4	-1.076	-1.25	O1W	-1.099	-1.28
Na1	0.970	0.94	H2W	0.581	0.64

kinetic energy density at the bond critical point (bcp) using Virial theorem [37,38]. The positive Laplacian values $\nabla^2\rho_{bcp}(r) > 0$, $|V|/G < 1$ show the closed shell type of interactions[39]. Among all the contacts, the OW-H1W...N3 and N2-H2N...O3 are the strongest hydrogen bonds according to distance, electron density and Laplacian values and are found to be $d = 1.1914(9) \text{ \AA}$, $1.901(10) \text{ \AA}$, $\rho = 0.189 \text{ e/\AA}^3$, 0.167 e/\AA^3 and $\nabla^2\rho_{cp} = 1.47 \text{ e/\AA}^5$, 3.14 e/\AA^5 respectively.

Atomic Charges

The experimental charges are derived from the basin atomic integration using VMOPro module [13] which are compared with the theoretical charges through AIM analysis. A good agreement is found between experimental and theoretical charges. The sulfur atom S1 bears the largest positive charge (EXP: 2.952 e, THEO: 3.06 e) since it is attached to the most electronegative O1 and O2 atoms [O1, EXP: -1.351 e, THEO: -1.34 e; O2, EXP: -1.389 e, THEO: -1.31 e] (Table 6). Notably, the bond S1-O2, which is formed by the most electronegative O2 atom and the most electropositive S1 atom, is more polarized compared to the S1-O1 bond. The methyl group (CH₃) which is attached to the electron withdrawing N1 atom has more positive

charge (+0.383 e) than the methyl group (0.212 e) which is attached to the C13 atom.

Electrostatic Potential and Reactivity Properties

The molecular electrostatic potential (MEP), is computed directly from the multipolar model using VMOPro tool with the help of the equation relating the electron density. The MEP isosurface at the 0.001 e/\AA^3 level of the electron density is shown in Figure 8. The O1 and O2 atoms are encapsulated with negative region (red in color) which is the most favorable site for electrophilic attack with the amino acid residues of the target protein.

The reactivity properties have been calculated from the gas phase calculation for the isolated molecule of meloxicam and meloxicam sodium monohydrate. The comparison of the reactivity properties of the meloxicam sodium monohydrate with its parent compound meloxicam shows that the salt monohydrate has more softness value than the pure compound. The comparison of reactivity properties of meloxicam and meloxicam sodium monohydrate have been given in Table 7. The energy gap of meloxicam sodium is comparatively lower (-0.099 a.u.) when it is compared to the energy gap of meloxicam

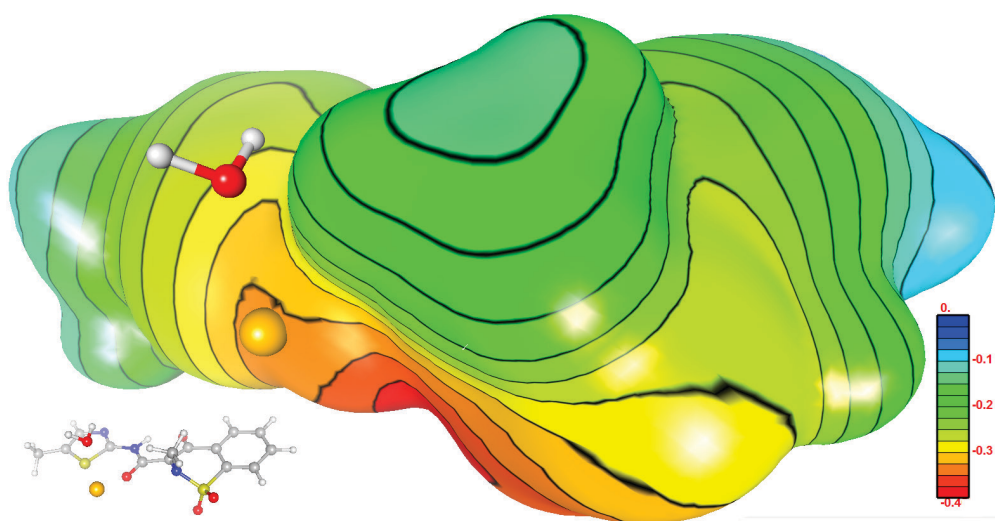


Figure 8. Isosurface of the meloxicam molecule at level $0.001 \text{ e}/\text{\AA}^3$ electron density. The surface is colored according to the electrostatic potential generated by the anion. The orientation of the molecule is also shown.

(-0.220 a.u.). This clearly shows that the molecule meloxicam sodium has high chemical potential, high kinetic stability and is a fast reacting ligand with the amino acid residues of the protein than the meloxicam compound.

Electrostatic Interaction Energy

The electrostatic interaction energies in the meloxicam sodium monohydrate crystal between neighboring moieties have been carried out (Table 8). Among the contacts, three different intermolecular contacts between the meloxicam anion (M) and the Na^+ anion are found with strong energies in the range -334 to -502 kJ/mol . In the strongest $\text{M}\cdots\text{Na}^+$ attractive electrostatic interaction, the sodium cation is in the vicinity of the SO_2 group and of the N1 tetragonal non-protonated nitrogen atom. In the two other $\text{M}\cdots\text{Na}^+$ interactions, the sodium cation is close to the $\text{C}=\text{O}$ carbonyl groups. The shortest distance between two Na^+ atoms is 3.787 \AA , which results in a repulsive energy of $+367 \text{ kJ/mol}$. Due to the global negative charge of meloxicam, all $\text{M}\cdots\text{M}$ dimers have positive repulsive electrostatic energy. The contribution of water molecules

appears secondary. Globally, the crystal is strongly maintained by the attractive $\text{M}\cdots\text{Na}^+$ interactions. The summation of the electrostatic energy of the asymmetric unit with all its direct neighbors yields a negative energy.

CONCLUSION

In this study, the charge density study of the anti-inflammatory drug meloxicam was determined from high resolution diffraction experiment at 90 K and is compared with the theoretical calculations for the gas phase of the molecule. The Hirshfeld surface analysis reveals that the ionic interactions $\text{O}\cdots\text{Na}^+$, the strong hydrogen bonds $\text{O}\cdots\text{H}/\text{n}$ and the hydrophobic contacts are the prime contributors to the crystal packing and are the most favored. The bond $\text{C}10-\text{O}4$ has the highest electron density value at the critical point which shows its strength among all the bonds. The sulfur atom has the largest positive charge because of its bonding with the two most electronegative O1 and O2 atoms, which enunciates that the bonds are highly polarized. The O1 and O2 atoms are

Table 7. Comparison of reactivity properties of meloxicam and meloxicam sodium monohydrate

Molecular descriptor	Meloxicam, Energy (a.u.)	Meloxicam Sodium Monohydrate, Energy (a.u.)
Electron affinity $A = [-E_{\text{LUMO}}]$	0.010	0.083
Ionization potential $I = [-E_{\text{HOMO}}]$	0.230	0.182
Global hardness $\eta = (I - A)/2$	0.066	0.049
Softness $S = 1/2\eta$	7.571	10.089
Electronegativity $\chi = (I + A)/2$	0.164	0.132
Electrophilicity index $\omega = \mu^2/2\eta$	0.204	0.176

Table 8. Electrostatic energy between interacting molecules in the meloxicam (M) sodium monohydrate crystal packing. Symmetry operator applies on the second moiety. In the summation, involution symmetry operators (inversions) were given a weight of ½.

Entities	Symmetry	E_{elec} (kJ/mol)
M··Na ⁺		-416
M··HOH	x, y, z	+2
Na ⁺ ··HOH		-72
M··M	$2-x, 2-y, 1-z$	+283
M··M	$2-x, 1-y, 1-z$	+131
M··HOH		-63
M··M		+311
M··Na ⁺	$1-x, 2-y, 1-z$	-502
Na··Na ⁺		+367
HOH··HOH	$1-x, 1-y, 1-z$	-2
M··Na ⁺	$1+x, y, z$	-334
M··HOH	$x, 1+y, z$	-91
M··M	$x, -1+y, 1+z$	+121
M··M	$-x+2, -y+3, -z$	+98
sum	neighbours	-478

highly prone to electrophilic attack with the amino acid residues of the target proteins. As the meloxicam compound exhibits global charge, the M··M dimers present in the crystal packing have positive repulsive electrostatic energy but the crystal is globally maintained by the electrostatic attractive M··Na⁺ ionic bridges. The electrostatic potential generated by the meloxicam anion is globally electronegative and is strongest around the SO₂ group. The reactivity studies clearly shows that the meloxicam sodium monohydrate has high chemical potential, softness, high chemical stability and is a fast interacting drug with the amino acid residues when compared to the meloxicam compound.

Supplementary Information. Supporting information to the paper is attached to the electronic version of the article at: <http://doi.org/10.5562/cca3346>.

REFERENCES

- [1] S. Noble, J. A. Balfour, *Drugs* **1996**, *51*, 424.
- [2] M. Ahmad, G. Murtaza, N. Akhtar, F. Siddique, S. A. Khan, *Acta Pol. Pharm. - Drug Res.* **2011**, *68*, 115.
- [3] R. D. Fleischmann, D. Alland, J. A. Eisen, L. Carpenter, O. White, J. Peterson, R. DeBoy, R. Dodson, M. Gwinn, D. Haft, E. Hickey, J. F. Kolonay, W. C. Nelson, L. A. Umayam, M. Ermolaeva, S. L. Salzberg, A. Delcher, T. Utterback, J. Weidman, H. Khouri, J. Gill, A. Mikula, W. Bishai, W. R. Jacobs, J. C. Venter, C. M. Fraser, *J. Bacteriol.* **2002**, *184*, 5479.
- [4] L. J. Crofford, *Arthritis Res. Ther.* **2013**, *15* Suppl 3, S2.
- [5] M. S. Carbone, C. I. Czimczik, T. F. Keenan, P. F. Murakami, N. Pederson, P. G. Schaberg, X. Xu, A. D. Richardson, *New Phytologist.* **2013**, *200*, 1145.
- [6] Rigaku Oxford Diffraction, CrysAlis PRO. Rigaku Oxford Diffraction, Yarnton, England, **2015**.
- [7] Bruker, APEX2, SAINT, TWINABS. Bruker AXS Inc., Madison, **2014**.
- [8] O. V. Dolomanov, L. J. Bourhis, R. J. Gildea, J. A. K. Howard, H. Puschmann, *J. Appl. Crystallogr.* **2009**, *42*, 339.
- [9] M. C. Burla, R. Caliandro, B. Carrozzini, G. L. Cascarano, C. Cuocci, C. Giacovazzo, M. Mallamo, A. Mazzone, G. Polidori, *J. Appl. Crystallogr.* **2015**, *48*, 306.
- [10] G. M. Sheldrick, *Acta Crystallogr. A* **2015**, *71*, s9.
- [11] C. B. Hübschle, G. M. Sheldrick, B. Dittrich, *J. Appl. Crystallogr.* **2011**, *44*, 1281.
- [12] N. K. Hansen, P. Coppens, *Acta Crystallogr. A* **1978**, *34*, 909.
- [13] C. Jelsch, B. Guillot, A. Lagoutte, C. Lecomte, *J. Appl. Crystallogr.* **2005**, *38*, 38.
- [14] Z. Su, P. Coppens, *Acta Crystallogr. A* **1998**, *54*, 646.
- [15] L. Kissel, B. Zhou, S. C. Roy, S. K. Sen Gupta, R. H. Pratt, *Acta Crystallogr. A* **1995**, *51*, 271.
- [16] A. Ø. Madsen, A. A. Hoser, *J. Appl. Crystallogr.* **2014**, *47*, 2100.
- [17] F. H. Allen, I. J. Bruno, *Acta Crystallogr. B* **2010**, *66*, 380.
- [18] S. Domagała, B. Fournier, D. Liebschner, B. Guillot, C. Jelsch, *Acta Crystallogr. A* **2012**, *68*, 337.
- [19] A. Thorn, B. Dittrich, G. M. Sheldrick, *Acta Crystallogr. A* **2012**, *68*, 448.
- [20] V. V. Zhurov, E. A. Zhurova, A. A. Pinkerton, *J. Appl. Crystallogr.* **2008**, *41*, 340.
- [21] P. Hohenberg, W. Kohn, *Phys. Rev.* **1964**, *136*, B864.
- [22] W. Kohn, L. J. Sham, *Phys. Rev.* **1965**, *140*, A1133.
- [23] R. G. Parr, W. Yang, *Density-Functional Theory of Atoms and Molecules*, Oxford University Press, New York, Oxford, **1989**.
- [24] A. D. Becke, *J. Chem. Phys.* **1993**, *98*, 5648.
- [25] C. Lee, W. Yang, R. G. Parr, *Phys. Rev. B* **1988**, *37*, 785.
- [26] M. J. Frisch, G. W. Trucks, H. B. Schlegel, G. E. Scuseria, M. A. Robb, J. R. Cheeseman, G. Scalmani, V. Barone, B. Mennucci, G. A. Petersson, H. Nakatsuji, M. Caricato, X. Li, H. P. Hrazchian, A. F. Izmaylov, J. Bloino, G. Zheng, J. L. Sonnenberg, M. Hada, M. Ehara, K. Toyota, R. Fukuda, J. Hasegawa, M. Ishida, T. Nakajima, Y. Honda, O. Kitao, H. Nakai, T. Vreven, J. A. Montgomery, Jr., J. E. Peralta, F. Ogliaro, M. Bearpark, J. J. Heyd, E. Brothers, K. N. Kudin, V. N. Staroverov, T. Keith, R. Kobayashi, J. Normand, K. Raghavachari, A.

- Rendell, J. C. Burant, S. S. Iyengar, J. Tomasi, M. Cossi, N. Rega, J. M. Millam, M. Klene, J. E. Knox, J. B. Cross, V. Bakken, C. Adamo, J. Jaramillo, R. Gomperts, R. E. Stratmann, O. Yazyev, A. J. Austin, R. Cammi, C. Pomelli, J. W. Ochterski, R. L. Martin, K. Morokuma, V. G. Zakrzewski, G. A. Voth, P. Salvador, J. J. Dannenberg, S. Dapprich, A. D. Daniels, O. Farkas, J. B. Foresman, J. V. Ortiz, J. Cioslowski, D. J. Fox, Gaussian, Inc., Wallingford CT, **2010**. Gaussian 09, Revision C.01.
- [27] T. A. Keith, T. K. Gristmill, AIMAll (Version 16.10.31), Software, Overland Park KS, USA, **2016**.
- [28] G. F. Fabiola, V. Bobde, L. Damodharan, V. Pattabhi, S. Durani, *J. Biomol. Struct. Dyn.* **2001**, *18*, 579.
- [29] R. Niranjana Devi, C. Jelsch, S. Israel, E. Aubert, C. Anzline, A. A. Hosamani, *Acta Crystallogr. B* **2017**, *73*, 10.
- [30] L. Chęcińska, S. Grabowsky, M. Małecka, A. J. Rybarczyk-Pirek, A. Józwiak, C. Paulmann, P. Luger, *Acta Crystallogr. B* **2011**, *67*, 569.
- [31] P. Śledź, R. Kamiński, M. Chruszcz, M. D. Zimmerman, W. Minor, K. Woźniak, *Acta Crystallogr. B* **2010**, *66*, 482.
- [32] G. Rajalakshmi, V. R. Hathwar, P. Kumaradhas, *Acta Crystallogr. B* **2014**, *70*, 568.
- [33] C. Jelsch, K. Ejsmont, L. Huder, *IUCrJ.* **2014**, *1*, 119.
- [34] R. N. Devi, M. G. Khrenova, S. Israel, C. Anzline, A. A. Astakhov, V. G. Tsirelson, *J. Mol. Model.* **2017**, *23*, 252.
- [35] D. Stalke, *Chem.-Eur. J.* **2011**, *17*, 9264.
- [36] P. Politzer, J. S. Murray, *Theor. Chem. Acc.* **2002**, *108*, 134.
- [37] R. F. W. Bader, *The Lagrangian Approach to Chemistry. The Quantum Theory of Atoms in Molecules*, Wiley-VCH Verlag GmbH & Co. KGaA. **2007**.
- [38] D. Cremer, E. Kraka, *Angew. Chem. Int. Edit.* **1984**, *23*, 627.
- [39] C. Gatti, *Z. Krist.-Cryst. Mater.* **2005**, *220*, 399.